

Proposal for the J-PARC 30-GeV Proton Synchrotron

Systematic investigation of the light kaonic nuclei – via the in-flight ${}^4\text{He}(K^-, N)$ reactions –

ver. June 22, 2020

H. Asano K. Itahashi, M. Iwasaki, Y. Ma, R. Murayama, H. Outa, F. Sakuma*,
T. Yamaga
RIKEN Cluster for Pioneering Research, RIKEN, Saitama, 351-0198, Japan

K. Inoue, S. Kawasaki, H. Noumi, K. Shirotori
*Research Center for Nuclear Physics (RCNP), Osaka University, Osaka, 567-0047,
Japan*

H. Ohnishi, Y. Sada, C. Yoshida
*Research Center for Electron Photon Science (ELPH), Tohoku University, Sendai,
982-0826, Japan*

T. Hashimoto
Japan Atomic Energy Agency (JAEA), Ibaraki 319-1195, Japan

M. Iio, S. Ishimoto, K. Ozawa, S. Suzuki
High Energy Accelerator Research Organization (KEK), Ibaraki, 305-0801, Japan

T. Akaishi
Department of Physics, Osaka University, Osaka, 560-0043, Japan

T. Nagae
Department of Physics, Kyoto University, Kyoto, 606-8502, Japan

H. Fujioka
Department of Physics, Tokyo Institute of Technology, Tokyo, 152-8551, Japan

M. Bazzi, A. Clozza, C. Curceanu, C. Guaraldo, M. Iliescu, M. Miliucci, A. Scordo,
D. Sirghi, F. Sirghi
Laboratori Nazionali di Frascati dell' INFN, I-00044 Frascati, Italy

P. Buehler, M. Simon, E. Widmann, J. Zmeskal
Stefan-Meyer-Institut für subatomare Physik, A-1090 Vienna, Austria

*Spokesperson, E-mail: sakuma@ribf.riken.jp

Abstract

We propose a series of experimental programs for the systematic investigation of the light kaonic nuclei, from the “ $\bar{K}N$ ” ($=\Lambda(1405)$) to “ $\bar{K}NNNN$ ”. Through the experiments, we provide the feature of the kaonic nuclei from the property changes depending on the mass number A , *i.e.*, nuclear density, which is related to spontaneous and explicit chiral symmetry breaking in QCD.

At the predecessor experiment (the J-PARC E15 experiment), we demonstrated the kaonic nuclei can be produced via the in-flight (K^- , N) reactions using the low-momentum DC kaon beam. The simplest kaonic nuclei, “ K^-pp ”, we observed has much deeper binding energy, compared to that of normal nuclei. We found that the large form factor obtained in a PWIA analysis implies the “ K^-pp ” state forms a quite compact and dense system.

For the next stage, we need to reveal the mass number dependence of the binding energy, decay width, and system size beyond the $\bar{K}NN$. On the other hand, when the mass number becomes large, it becomes difficult to handle the number of particles in the final state and to deduce the physics behind it. Thus, we take a step-by-step approach. In this proposal, we are aiming to measure the $\bar{K}NNN$ ($A = 3$) system as a first step toward the comprehensive study. From the experience of E15, we have learned that reducing the number of particles in the final state is the key to remove ambiguity to interpret the reaction process. Therefore, we focus on $K^-ppn \rightarrow \Lambda d$ and Λpn decay channels in ${}^4\text{He}(K^-, \Lambda d/\Lambda pn)n$ reactions.

To realize the systematic measurements, a large acceptance spectrometer and the high-intensity kaon beam are mandatory. We are planning to construct a new 4π cylindrical detector system (CDS) to drastically enlarge the acceptance to detect all the particles in the final states. It enables us to specify the reaction channel unambiguously. We also propose to improve the K1.8BR beamline spectrometer by shortening the beamline to utilize $\sim 40\%$ more K^- than the previous configuration.

Summary of the proposed experiment

beamline:	K1.8BR
Primary beam:	30 GeV, 90kW (5.2 s spill interval)
Secondary beam:	1.0 GeV/ c K^-
Beam intensity:	3.2×10^5 on target per pulse
Reaction:	in-flight (K^- , N)
Detectors:	improved K1.8BR beamline spectrometer, and new cylindrical detector system
Target:	Liquid ^4He
Beam time:	1 week for commissioning, 1 week for performance study with H_2 target, and 3 weeks for the physics run with ^4He target
Estimated yield:	1.9×10^4 $K^-ppn \rightarrow \Lambda d$, and 2.8×10^3 $K^-ppn \rightarrow \Lambda pn$

1 Introduction

The study of the $\bar{K}N$ interaction is one of the most important subjects to understand meson-baryon interactions in low energy quantum chromodynamics (QCD). Extensive measurements of anti-kaonic hydrogen atom [1–3] and low-energy $\bar{K}N$ scattering [4] have revealed the strongly attractive nature of the $\bar{K}N$ interaction in the isospin $I = 0$ channel. As a consequence, possible existence of deeply-bound kaonic nuclear states has been widely discussed [5–24].

Among the kaonic nuclei, the $\bar{K}NN$ system with $I = 1/2$ and $J^P = 0^-$ (symbolically denoted as “ K^-pp ”) is of special interest because it is the lightest $S = -1$ \bar{K} nucleus and whose existence is supported by many theoretical works today. Over the past 20 years, the existence of the “ K^-pp ” was not been established despite of many experimental efforts. Several groups reported an observation of a “ K^-pp ” candidate with the binding energy of around 100 MeV, in experiments which measured non-mesonic decay branches of Λp and/or $\Sigma^0 p$ in different reactions [25–27]. On the other hand, there are contradicting reports concluding that the reactions can be understood without a bound state [28–31]. Recently, the J-PARC E15 experiment pinned down the existence of the “ K^-pp ” bound state by using the simplest reaction of in-flight ${}^3\text{He}(K^-, N)$ [32–34]. A distinct peak structure was observed well below the mass threshold of $K^- + p + p$ in the Λp invariant-mass spectrum, obtained from the ${}^3\text{He}(K^-, \Lambda p)n$ measurement. The simplest and natural interpretation of this peak is a kaon-nuclear bound-state, “ K^-pp ”. This result is experimentally solid as against the previously reported results, thus the existence of the “ K^-pp ” bound state is experimentally clarified.

The state of the kaonic nuclei is predicted to be compact due to the strong attraction of the $\bar{K}N$, which indicates that the high-density nuclear matter is realized in the system. In deed, the E15 results give us an insight that the “ K^-pp ” could be quite compact system comparing to the mean nucleon distance of normal nuclei. By expanding this study to more heavier systems, we can conduct a systematic investigation of the system size via the form factor measurement, especially momentum transfer dependence on the mass number. Theoretical calculations on the system size utilizing different $\bar{K}N$ interaction models are still limited, so it is very important to initiate the study by experimental approaches.

In particular, the $A = 4$ system of $\bar{K}NNNN$ is important to address the system size of the kaonic nuclei. Due to the repulsive force between nucleons, the state of the $\bar{K}NNNN$ would be formed when the \bar{K} is placed into the center of the $NNNN$ system, where the nucleons can form an α particle configuration. Such three-dimensional and quite symmetric configuration can only be realized in the system, therefore the state is extremely interesting and having great importance. On the other hand, from the experimental point of view, it becomes difficult to handle number of particles in the final state when the mass number becomes large. Thus, we take a step-by-step approach in the series of experimental programs.

At the K1.8BR beamline, a series of experimental programs has been planned to aim a systematic investigation of the kaonic nuclei in light nuclei, *i.e.*, from the

“ $\bar{K}N$ ” ($=\Lambda(1405)$) to “ $\bar{K}NNNN$ ”. The experimental series is realized by using the world’s highest intensity of low-momentum kaon beam at J-PARC. The programs mainly consist of:

- Precise measurement of the $\Lambda(1405)$ state in large momentum transfer region via the $d(K^-, n)$ reaction, to experimentally clarify the picture whether it is a baryonic state or a $\bar{K}N$ molecular state,
- Investigation of the spin and parity of the $\bar{K}NN$ state via the ${}^3\text{He}(K^-, N)$ reactions,
- Search for the $\bar{K}NNN$ states via the ${}^4\text{He}(K^-, N)$ reactions, as for the bridge to access heavier system, and,
- Advanced search for the $\bar{K}NNNN$ states via the ${}^6\text{Li}(K^-, d)$ reaction.

In parallel to these studies, we also wish to access the $S = -2$ kaonic nuclei such as the theoretically predicted K^-K^-pp state, as we previously submitted an Letter-of-Intent to J-PARC. The $\bar{K}\bar{K}NN$ system could give us a chance to access even higher density than the $S = -1$ kaonic nuclei. As we submitted the LoI, one possible way for the measurement at J-PARC is:

- Search for the $\bar{K}\bar{K}NN$ states via the $\bar{p} + {}^3\text{He}$ annihilation.

To realize this experiment, a 4π spectrometer is essential to study the basic elementary cross section of the annihilation which is needed to be clarified to design the feasible experiment. The production cross sections of the $\bar{K}\bar{K}NN$ states are considered to be quite small – roughly one-thousandth of those of the $S = -1$ kaonic nuclei.

For the systematic and precise measurements, we are planing to construct a totally new 4π spectrometer to measure all particles involved in the reactions and to reconstruct its formation and decay exclusively. The spectrometer is designed to keep high versatility that all the experiments can be performed by changing the target materials. In addition, to use the high-intensity kaon beam more efficiently, we propose to shorten the existing K1.8BR beamline for larger kaon yield without deteriorating the momentum resolution of the kaon beam.

In the proposal, we evaluate the required beam time to conduct an experimental search for the $\bar{K}NNN$ bound state for the first step, to accomplish the systematic investigation of the light kaonic nuclei. Besides this proposal, we are now preparing the other new proposals for the precise investigation of the $\bar{K}NN$ system using ${}^3\text{He}$ target. Utilizing the asymmetry of the decay in terms of Λ spin and resulting polarized proton, we are going to measure the analyzing power of the proton spin at the secondary scattering on the hodoscope around $500\text{ MeV}/c$. This information, which is not available at present, is inevitable to design the successive experiment to measure the angular distribution of the decay products, and to pin down the spin-parity assignment of the kaonic nuclei. The other challenging experiments – $\Lambda(1405)$ production in large

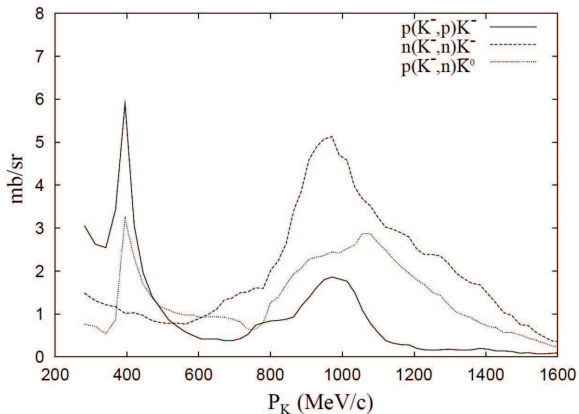


Figure 1: Cross sections of the $\bar{K}N \rightarrow \bar{K}N$ reactions at $\theta_n = 0$ (neutron forward / kaon backward) [35].

momentum transfer region and the $\bar{K}NNNN/\bar{K}\bar{K}NN$ bound state search – will also be proposed in the near future.

We introduce an overview of the “ K^-pp ” measurement at the E15 experiment in the rest of this section to show what we have learned from the modern experimental investigation dedicated to the kaonic nuclei. Then we show the details of the proposed experiment focusing on the $\bar{K}NNN$ search in Sec.2 and subsequent sections.

1.1 Results of the E15 Experiment

We conducted an experimental investigation of the “ K^-pp ” bound state using the simplest \bar{K} induced reaction of $K^- + {}^3\text{He}$ via the nucleon knock-out reactions $\bar{K}N \rightarrow \bar{K}'N$ followed by two nucleon absorption of $\bar{K}' + NN \rightarrow “K^-pp”$. In the experiment, we used the kaon momentum of 1 GeV/c where the $\bar{K}N \rightarrow \bar{K}N$ reactions have the maximum cross section as shown in Fig 1. The recoiled kaon ‘ \bar{K} ’ at a momentum q behaves as a ‘off-shell particle’ (total energy can be lower than its intrinsic mass) within a time range what the uncertainty principle allows. The momentum transfer q is defined between the incident kaon and the outgoing neutron in the laboratory frame $q = |\mathbf{p}_{K^-}^{lab} - \mathbf{p}_n^{lab}|$. In the reaction, we utilized this low-momentum back-scattered kaon as a ‘off-shell kaon’ source and residual spectator nucleons NN as an ‘actual target’ to form a “ K^-pp ” state, whose energy is below their intrinsic mass of $M(Kpp)$ ($= m_K + 2m_N = 2.37 \text{ GeV}/c^2$).

With the Λpn final states, we observed a kinematic anomaly in the Λp invariant mass near the mass threshold of $M(Kpp)$ at around $q \sim 0.4 \text{ GeV}/c$ [33,34]. As shown in Fig. 2 (left), we confirmed the existence of the bound state below the mass threshold of $M(Kpp)$, whose mass centroid is independent on q , at as deep as the binding energy of $\sim 50 \text{ MeV}$ [34]. The back-scattered ‘on-shell’ kaon, whose total kaon energy is above its intrinsic mass, can also be absorbed by the spectator nucleons without forming a

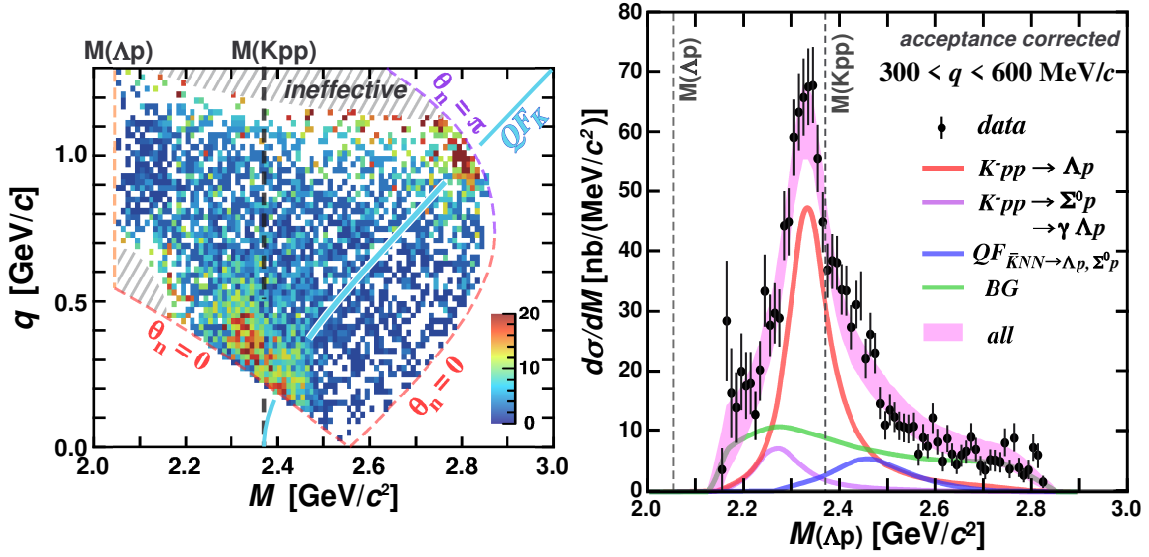


Figure 2: (left) Efficiency and acceptance corrected data over M (Λp invariant mass) and q (momentum transfer). (right) The Λp invariant mass in the region of $0.3 < q < 0.6 \text{ MeV}/c$.

bound state. The kinematical centroid of such quasi-free absorption process is plotted in the figure, denoted as QF_K . Along the line, there are two event concentration points at $\theta_n = 0$ and $\theta_n = \pi$, but both are well separated from the region of interest. Figure 2 (right) shows the acceptance and efficiency corrected Λp invariant mass in the region of $0.3 < q < 0.6 \text{ GeV}/c$, where the “ K^-pp ” bound state is dominant. A clear peak originated from the “ K^-pp ” can be seen below $M(Kpp)$, whose binding energy reaches to $\sim 50 \text{ MeV}$. We also excluded any possibility to form a spurious structure in the Λp invariant mass spectrum. Thus the simplest and natural interpretation is a kaon-nuclear bound state “ K^-pp ”. The structure below the mass threshold in the Λp spectrum obtained has also been theoretically interpreted as the $\bar{K}NN$ quasi-bound system [21, 36]. The experimental spectrum can be reproduced with the $\bar{K}NN$ quasi-bound system and the quasi-free processes based on theoretical treatment of the ${}^3\text{He}(K^-, \Lambda p)n$ reaction.

The observed large form factor of $\sim 400 \text{ MeV}/c$ based on the simple plane wave impulse approximation (PWIA) and the large binding energy of the “ K^-pp ” state imply the formation of a quite compact and dense system. To deduce the size information, more sophisticated studies on reaction dynamics are needed both theoretically and experimentally.

Then a question arises whether or not the “ K^-p ” bound state is also produced in the same $K^- + {}^3\text{He}$ reaction. The $\Lambda(1405)$ state with $I = 0$, which locates slightly below the $\bar{K}N$ mass threshold and decays into $\pi\Sigma$, is theoretically considered as a quasi-bound state of $\bar{K}N$ in the $I = 0$ as supported by lattice QCD calculation [37]. Based on this consideration, the production mechanism of the $\bar{K}NN$ system is assumed

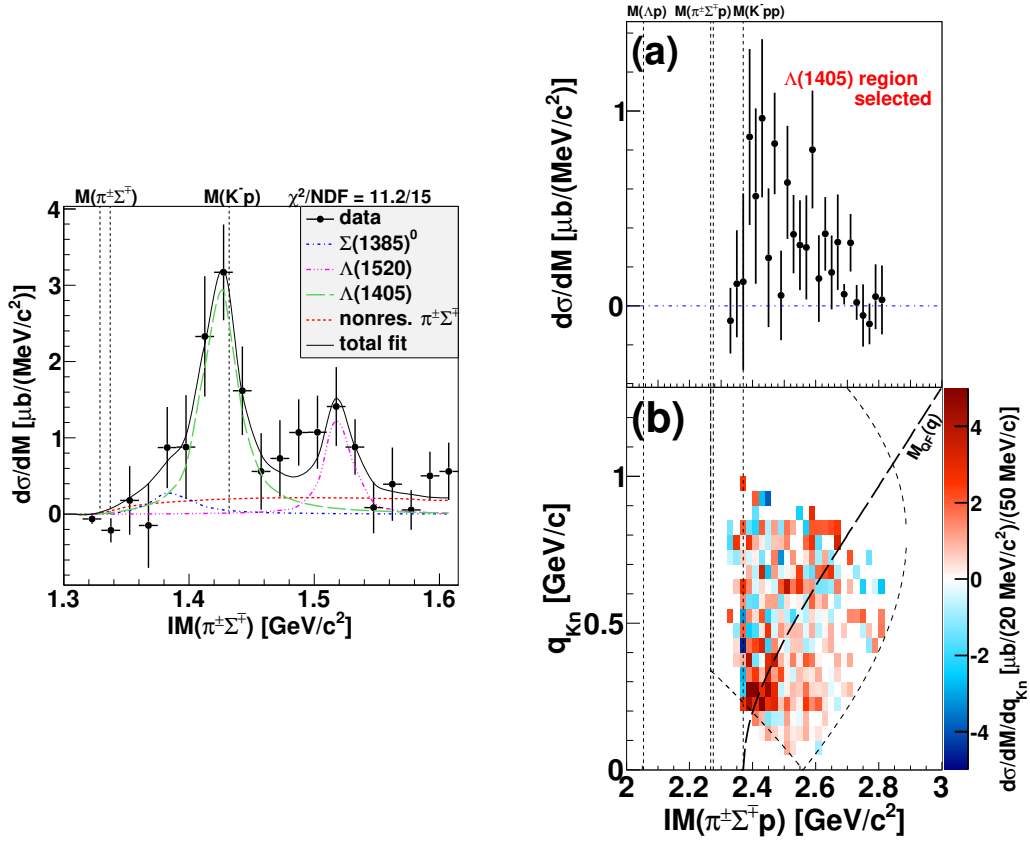


Figure 3: (left) Efficiency and acceptance corrected $\pi^\pm\Sigma^\mp$ invariant mass in the $\pi^\pm\Sigma^\mp pn$ final state. The spectrum is fitted with $\Sigma(1385)$, $\Lambda(1405)$, $\Lambda(1520)$ and quasi-free $\pi^\pm\Sigma^\mp$ background. (right) (a) Efficiency and acceptance corrected $\pi^\pm\Sigma^\mp p$ invariant mass and (b) q versus $IM(\pi^\pm\Sigma^\mp p)$ in the $\Lambda(1405)$ region. In (b), the kinematical quasi-free function $M_{QF}(q)$ of $K^-N \rightarrow \bar{K}n$ followed by $\bar{K}NN \rightarrow \Lambda(1405)p$ is also plotted.

with a $\Lambda(1405) + N \rightarrow \bar{K}NN$ doorway process in theoretical models [38]. Hence, an investigation of the $\Lambda(1405)$ production in the $K^- + {}^3\text{He}$ reaction is crucial together with the “ K^-pp ” production.

From our recent analysis of an exclusive measurement of the $\Lambda(1405)$ state produced in the reaction $K^- + {}^3\text{He} \rightarrow Y^{*0} + p + n$, an important hint of the production mechanism of the “ K^-pp ” bound state has been obtained. Figure 3 (left) shows the invariant-mass spectrum of $\pi^\pm\Sigma^\mp$ in the $\pi^\pm\Sigma^\mp pn$ final states. The $\Lambda(1405)$ state is clearly identified, whose cross section of $\sim 200 \mu\text{b}$ has been obtained by simple Breit-Wigner fit. By comparing the obtained “ K^-pp ” $\rightarrow \Lambda p$ cross section of $\sim 10 \mu\text{b}$, the production of the $\Lambda(1405)$ is ~ 10 times large. Then the $\Lambda(1405)pn$ final state can be selected with the region around the $\Lambda(1405)$, which can be compared to Λpn final state. The $\pi^\pm\Sigma^\mp p$ invariant-mass spectrum in the $\Lambda(1405)$ region is shown in Fig. 3 (right). One can see

that the $\Lambda(1405)pn$ events distribute above the $M(Kpp)$ mass threshold in the $\pi^\pm\Sigma^\mp p$ invariant-mass spectrum. The curve originating at $M = M(Kpp)$ in Fig. 3 (right)(b) represents the kinematical centroid of the quasi-free absorption process M_{QF} , as with the case of the Λpn final state. The curve reproduces the q -dependence of the event distribution rather well not only in the small q region around 0.3 GeV/ c but also in the large q region around 0.7 GeV/ c . Therefore, the result strongly indicates that the $\Lambda(1405)$ is produced via the quasi-free processes followed by the two-nucleon absorption process.

On the other hand, the structure below the mass threshold can not be seen where we found the “ K^-pp ” state in the Λp spectrum. From a theoretical point of view, the $\bar{K}NN$ is a resonant state in the $\bar{K}NN - \pi\Sigma N - \pi\Lambda N$ coupled-channel system, hence the mesonic $\pi\Sigma N$ decays are expected to be dominant compared to the non-mesonic ΛN decay [39]. However, the experimental result indicates small $\pi\Sigma N$ -decay branch of the “ K^-pp ” bound state. This discrepancy can be naively interpreted using the decay phase-space volume of the “ K^-pp ”. The $\pi\Sigma N$ -decay phase space below the $M(Kpp)$ mass threshold is kinematically limited in the $\pi\Sigma$ decay, while the Λp -decay phase space has no limitation reaching to ~ 300 MeV/ c^2 below $M(Kpp)$. Therefore, the decay branches into non-mesonic YN channels would be widely opened when the “ K^-pp ” bound state is formed. This interpretation is consistent with our observation of the “ K^-pp ” in the Λp channel; the obtained width of ~ 100 MeV is larger than theoretical expectations considering only the mesonic $\pi\Sigma N/\pi\Lambda N$ decays.

It can also be interpreted by considering the scattered-kaon energy of the first-step $K^-N \rightarrow \bar{K}'n$ process in the laboratory frame (E_K^{lab}) as follows.

- When the scattered-kaon energy is above its intrinsic mass m_K ($E_K^{lab} > m_K$), the ‘ $\bar{K}' + NN \rightarrow \Lambda(1405)p$ ’ reaction is dominant compared to the Λp channel. One possible reaction mechanism of this process can be considered as follows. The scattered kaon knocks out a residual proton to which the energy-momentum mismatch is transferred, and the kaon is successively absorbed in the other residual nucleon mainly as ‘off-shell kaon’ resulting the “ K^-p ” bound-state ($\Lambda(1405)$) formation. This two-nucleon-involved reaction could be reflected by the strongly attractive $\bar{K}N$ interaction.
- On the other hand, when the kaon energy is below the intrinsic mass ($E_K^{lab} < m_K$), the “ K^-pp ” bound state is formed via the ‘ $\bar{K}' + NN \rightarrow “K^-pp”$ ’ reaction. The “ K^-pp ” is produced via ‘ \bar{K}' ’ capture by two residual nucleons with the energy-momentum match condition. In the region below $M(Kpp)$, the non-mesonic YN decays are widely open due to the phase space limitation of the $\pi\Sigma N$ decays.

Thus, the E15 experiment opened a new era of experimental research on the kaonic nuclei with the virtual kaon beam produced from the in-flight (K^-, N) reactions. This was realized by using the world’s highest intensity kaon beam available at J-PARC. On the other hand, we found several difficulties to proceed with further investigations of the kaonic nuclei with the existing setup. In the series of the new experiments,

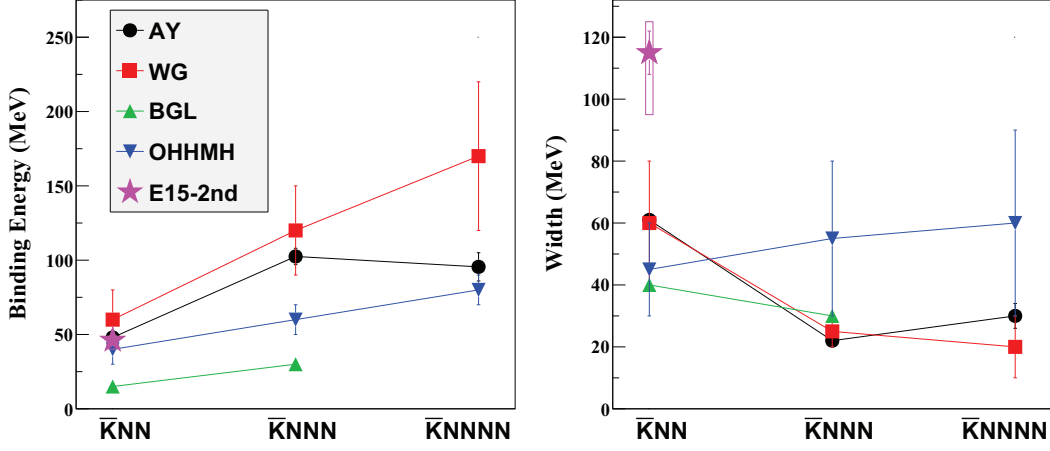


Figure 4: Summary of the theoretical calculation of kaonic nuclei in light nuclei from $A = 2$ to 4 in different models AY [6, 7], WG [13], BGL [16], and OHHMH [22]. The result obtained at the E15-2nd experiment is also plotted [34].

we continue the systematic researches on the light kaonic nuclei by using a new large acceptance detector system and the improved K1.8BR beamline.

2 Purpose of the Proposed Experiment

The final physics goal of the experiment we proposed is to reveal \bar{K} meson property inside nuclei via the $\bar{K}N$ interaction. The meson-baryon interactions close to the mass thresholds are known to provide crucial information on spontaneous and explicit chiral symmetry breaking. Among meson-baryon interactions, $\bar{K}N$ interaction is a powerful probe to understand this important aspect of low energy QCD. On the other hand, investigations of the $\bar{K}N$ interaction are quite complicated and thus challenging, due to the presence of the $\Lambda(1405)$ state located just below the $\bar{K}N$ mass threshold. The $\Lambda(1405)$ state is theoretically considered as a quasi-bound state of $\bar{K}N$. One of the straightforward methods to reveal the interaction below the $\bar{K}N$ mass threshold is to perform a precise measurement on the line shape of this $\Lambda(1405)$ state with the $\bar{K}N \rightarrow \pi\Sigma$ channels, as we demonstrated at the E31 experiment. The analysis is in progress, and final results will come out shortly.

At the same time, based on the consideration that the $\Lambda(1405)$ to be a bound state of $\bar{K}N$, the possible existence of kaon-nuclear quasi-bound states has been widely discussed. The properties of the kaonic nuclei strongly depend on the $\bar{K}N$ interaction. Thus the systematic investigation of the kaonic nuclei will also provide the new insight on the $\bar{K}N$ interaction below the mass threshold.

The binding energy and decay width mainly characterize the property of the kaonic

nuclei. The system size dependence has been calculated with several theoretical models, as summarized in Fig. 4. The predicted values of the binding energy and decay width are scattered out widely due to the difference of the $\bar{K}N$ interaction models. Still, almost of all predictions show that the larger size nuclei have the larger binding energy. As for the width, the theoretical calculations take into account only mesonic decay channels, including $\pi\Sigma$ and $\pi\Lambda$. Thus, the calculated width would become large if the models adopt non-mesonic decay channels, as demonstrated in Ref. [17].

In the proposed experiment, we focus on an investigation of the kaonic nuclei with mass number $A = 3$, *i.e.*, $\bar{K}NNN$. The experimental results provide the first steps on the system size dependence of the $\bar{K}N$ interaction. The dependence reveal the $\bar{K}N$ interaction below the mass threshold by comparing the obtained properties of the $\bar{K}NNN$ state with those of the previously reported “ K^-p ” ($=\Lambda(1405)$) and “ K^-pp ” states.

3 Experimental Method and Apparatus

Up to the present, the $\bar{K}NNN$ state has been mainly searched for with stopped K^- reactions. The KEK-PS E471/E549 collaborations measured the inclusive ${}^4\text{He}(K^-_{\text{stopped}}, p/n)$ reactions with a spectrometer dedicated to TOF measurement of protons and neutrons [40, 41]. They found no specific peak structures below the mass threshold of $M(\bar{K}NNN)$ in the missing mass spectra from the reactions. This is due to huge backgrounds originated from the two nucleon absorption processes, $\bar{K}NN \rightarrow YN$, and quasi-free hyperon productions and its decays, $\bar{K}N \rightarrow \pi Y$, whose production mechanisms are quite complicated in the stopped K^- reactions. The backgrounds can not be discriminated kinematically from the signal with small production cross section in the inclusive measurement. Indeed, with the inclusive analysis of the in-flight ${}^3\text{He}(K^-, n)X$ measurement, we found no significant peak structure due to the huge backgrounds from quasi-free processes and the two nucleon absorption processes [32]. By reducing the backgrounds with the exclusive measurement of ${}^3\text{He}(K^-, \Lambda p)n$ and identifying all the final-state particles in wide momentum-transfer region, the “ K^-pp ” signal was able to be separated from the backgrounds in large momentum-transfer region. The “ K^-pp ” signal has much smaller cross section ($\sim 10 \mu\text{b}$) compared to the quasi-free processes ($\sim 10 \text{mb}$), and distributes up to $q \sim 600 \text{MeV}/c$ [33, 34].

On the other hand, there are two reports of observation of the “ K^-ppn ” candidates below the mass threshold in the Λd invariant mass spectrum with the stopped K^- reactions (FINUDA) and the heavy-ion collisions (FOPI). The FINUDA collaboration reported that the candidate has the binding energy of $\sim 60 \text{MeV}$ and the width of $\sim 40 \text{MeV}$ as shown in Fig. 5 (left) [42]. The candidate reported from the FOPI collaboration has much deeper binding energy of $\sim 150 \text{MeV}$ with broader width of $\sim 100 \text{MeV}$, as shown in Fig. 5 (right) [43]. However, because these measurements were performed only inclusively, possible contributions of multi-nucleon absorption process and intermediate states of N^*/Y^* to the peak structure can not be excluded. Besides,

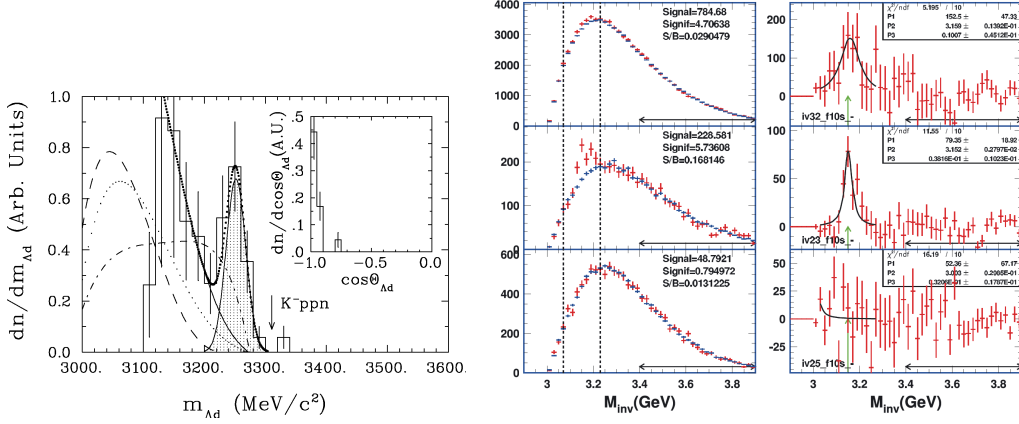


Figure 5: Invariant mass spectra of Λd reported from (left) the FINUDA collaboration in the ${}^6\text{Li}(K_{\text{stop}}^-, \Lambda d)3N$ reaction [42] and (right) the FOPI collaboration in the Ni+Ni reaction at 1.93 AGeV [43].

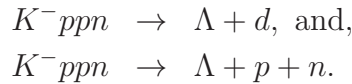
those statistics reported were very limited, thus the results still remain speculated as of today.

Therefore, the key to the experimental search is to adopt a simple in-flight reaction and to measure it exclusively. Simple in-flight reaction, such as in-flight \bar{K} induced reactions with light target nuclei, enables us to specify the reaction channel using the momentum-transfer dependence. Exclusive measurement is crucial to distinguish a small and broad signal from largely and widely distributed quasi-free and multi-nucleon absorption backgrounds.

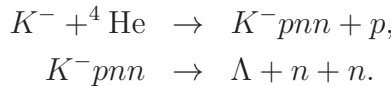
In the proposed experiment, we perform the exclusive measurements of the production and decay of the “ K^-ppn ” state using



reaction followed by expected no-mesonic decays of



We determine the binding energy and the width from the invariant mass reconstruction of the decays. The invariant mass is obtained as a function of the momentum transfer to distinguish the bound-state production from the quasi-free processes and multi-nucleon absorption processes by the event kinematics as demonstrated in the E15 analysis. In the same $K^- + {}^4\text{He}$ reaction, it can be possible to measure the isospin partner of “ K^-ppn ”, *i.e.*, the “ K^-pnn ” state via



Comparison of the properties between the isospin partners is of special importance to investigate the internal composition of the kaonic nuclei. On the other hand, the measurement is experimentally challenging, because two neutron detection is required to identify the K^-pnn decay.

We realize the $\bar{K}NNN$ production using the (K^-, N) reaction at the K1.8BR beamline, as successfully performed in the previous experiment E15; a recoiled virtual kaon (\bar{K}') generated by $K^-N \rightarrow \bar{K}'n$ processes can be directly induced into residual nucleons within the strong interaction range. We utilize 1.0 GeV/ c incident kaon to maximize $\bar{K}N$ reaction rate at zero degree as shown in Fig.1. Incoming K^- beam is identified and its momentum is analyzed by the beamline spectrometer. The beam kaon is irradiated to the targets located at the final focus point, and the all particles generated from the reactions are identified with a cylindrical detector system (CDS) that surrounding the target system. The kaonic nuclei are identified via invariant-mass reconstruction of the decay particles. By detecting the nucleon coming from the initial (K^-, N) reactions, or by identifying that with missing mass technique, we realize exclusive measurement of the production of the kaonic nuclei.

The details of each apparatus used for the experimental programs, including the existing system, are described in the following sub-sections.

3.1 Beamline Spectrometer

We are planning to conduct the new experiment at the K1.8BR beamline. For the new experiment, we propose a new configuration of the beamline to achieve efficient utilization of the K^- beam. By this new setup, the available kaons on target are expected to increase by ~ 1.4 times compared to the current beamline configuration, which corresponds to 3.2×10^5 kaons on target per spill at the beam power of 90 kW with a 5.2 s repetition cycle.

The beamline spectrometer is composed of beamline magnets, trigger counters, beam trackers, and a kaon identification counter [44, 45]. The beam TOF measurement is performed with a newly developed beam hodoscope tracker (BHT) installed at the just upstream of the D4 magnet and a T0 counter after D4. Kaon beams are identified with an aerogel Cherenkov counter whose reflective index is 1.05. The kaon beam is tracked with the BHT and a beamline chamber, and the momentum of the beam is analyzed with this tracking information together with the beam optics of the D4 magnet. The expected momentum resolution is 2×10^{-3} , which was the same resolution achieved at the predecessor experiments. We also use a beam definition counter (DEF) installed just upstream of the target cell to suppress the trigger rate. We can utilize the existing apparatus at the current K1.8BR beamline except for the BHT. We plan to construct the BHT using an array of thin plastic scintillator slab ($3 \sim 5[W] \times 3[T] \times 150[H]$ mm) with MPPC readout.

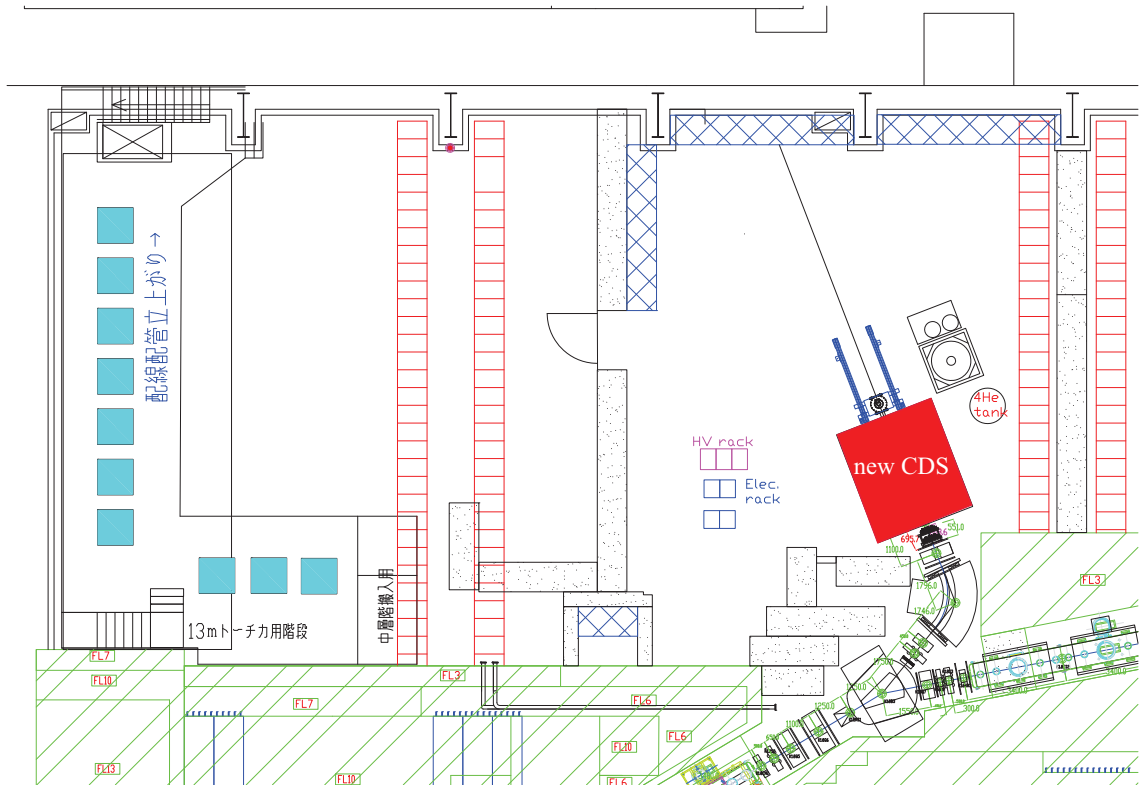


Figure 6: Plan of a layout of the K1.8BR experimental area for the proposed experiment.

3.2 Target System

As discussed above, the main target nucleus for the proposed experiment is ${}^4\text{He}$. To realize a reasonable reaction rate, we use liquid ${}^4\text{He}$ as the target. We use a pulse tube refrigerator system developed for the hyper triton measurement (J-PARC P73 experiment). The system has the capability to liquefy all types of $\text{H}_2/\text{D}_2/{}^3\text{He}/{}^4\text{He}$ gases with the same system. Figure 7 shows a schematic view of the target system for the P73 setup. We modify the system to be dedicated to the newly constructed CDS. In the proposed experiment, a pure beryllium target cell developed for E15 is used, whose dimension is 6.8 cm in diameter and 13.7 cm in length.

The target system has been successfully operated at the K1.8BR beamline. The achievable temperature of the system is 2.7 K, in which the density of the liquid ${}^4\text{He}$ is 0.144 g/cm^3 with a stability of better than 0.1%.

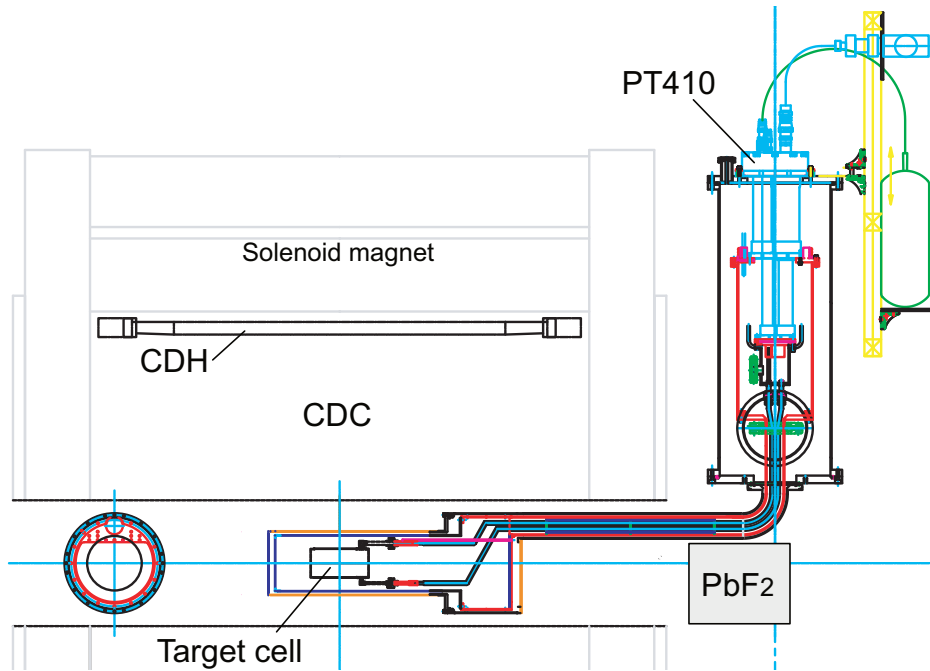


Figure 7: Schematic view of the target system at the K1.8BR beamline. The figure shows the setup for the P73 experiment. We modify the system for the proposed experiment by changing a transfer chamber located between a main cryogenic chamber and a target chamber.

3.3 Cylindrical Detector System (CDS)

Efficient and high precision reconstruction of decay particles from the target region with large acceptance is a key for the proposed experiment. To this end, we newly construct a large size CDS at the K1.8BR beamline. The requirements for the CDS are as follows:

4π acceptance

The exclusive measurement of the (K^-, N) reactions is essential for the experiment. To detect particles involved in the reaction as much as possible, the detector acceptance needs to be substantially identical to 4π , for both of charged and neutral particles coming from the target region. The large acceptance system can reduce backgrounds attributed to particle misidentification from missing particles.

High resolution

The spacial and timing resolution of the detector system has to be as good as possible to precisely reconstruct the decays of the kaonic nuclei and to determine its properties. At minimum, the resolution achieved with the previously used

CDS is required to efficiently reconstruct the $\Lambda \rightarrow \pi^- p$, $\Sigma^\pm \rightarrow \pi^\pm n$, and $K^0 \rightarrow \pi^+ \pi^-$ decays.

Neutral-particle detection

Detection of neutral particles from the production and decay is of special importance in the proposed experiment. Especially, large detection efficiency for neutron is a key in the series of the experimental programs. In reconstruction of the sequential decay of $\Lambda(1405) \rightarrow \pi^\pm \Sigma^\mp$ followed by $\Sigma^\pm \rightarrow \pi^\pm n$, the decay neutron has low momentum of a few 100 MeV/ c . Thus we have to measure the neutron with time-of-flight technique using a plastic scintillator which is the best way of the low-momentum neutron measurement. A electromagnetic calorimeter is also an essential apparatus to measure the $\Sigma^0 \rightarrow \gamma \Lambda$ decay. The pure $I = 0$ channel of the $\Lambda(1405) \rightarrow \pi^0 \Sigma^0$ is the most important channel to deduce the spectral shape of the $\Lambda(1405)$.

To fulfill the requirements described above, the CDS is designed to be composed of five main subsystems: a superconducting solenoid magnet, a cylindrical drift chamber (CDC), backward and forward drift chambers (BDCs/FDCs), a neutron counter (NC), and an electromagnetic calorimeter (ECAL). A conceptual design of the CDS is shown in Figs. 8 and 9. Design of each detector component is described in the following subsections.

The component of the CDS would be easily rearranged to be dedicated to individual experimental aims. For instance, to measure the polarization of the decay Λ and proton from the “ $K^- pp$ ” state for the spin determination, we are planing to install a polarimeter composed thin plastic scintillators and a tracker system by replacing the NC (and the ECAL). Details of “the $K^- pp$ project” will be shown in the other proposal in the near future. The installation of such tracker system also enables us to perform high precision measurement of charged decay modes of the kaonic nuclei with a few MeV/ c^2 mass resolution, thanks to large lever arm length of the tracking volume.

3.3.1 Superconducting Solenoid Magnet

In the proposed experimental programs, we adopt almost the same design of ‘the detector solenoid magnet’ of the COMET experiment developed by the KEK Cryogenic Science Center. The magnet provides a uniform field strength inside the tracking volume whose strength we use is 0.7 T at the center of the magnet [†].

The magnet uses the Ni-Ti-Cu superconductor with three GM refrigerators, and is operated with a 80 kVA power supply (AC415V - 200A). The bore diameter of the magnet is 1.8 m and length is 3.3 m with an overall weight of ~ 25 tons. The shape of the return yoke is square shape whose external dimensions is 3.4 m \times 3.4 m \times 3.9 m.

[†]The solenoid magnet is designed to be able to provide the magnetic field of 1.0 T for the COMET experiment.

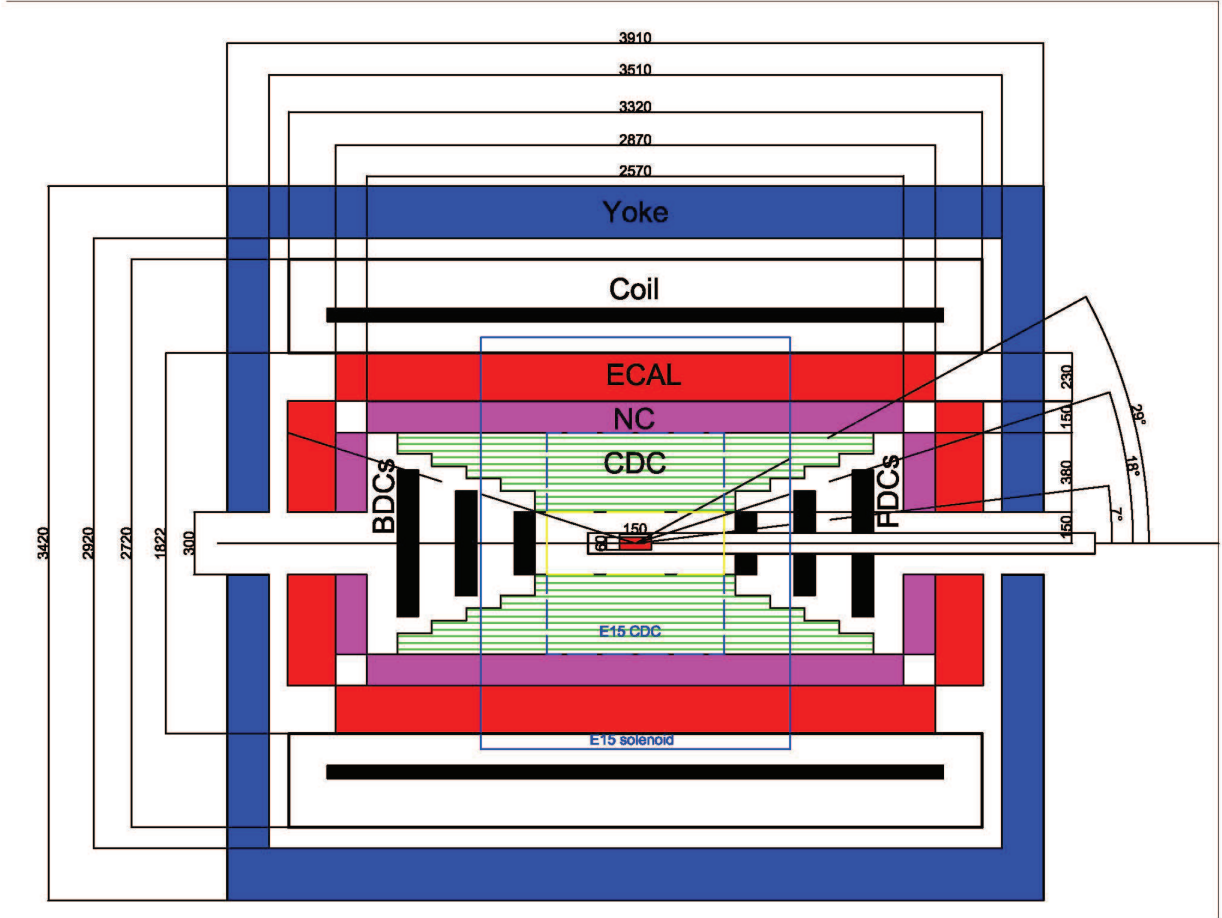


Figure 8: Conceptual design of the CDS (cross section).

3.3.2 Cylindrical Drift Chamber (CDC)

The conceptual design of the CDC is shown in Fig. 10. The CDC is designed to be symmetric in the z direction (beam direction) to provide a $29^\circ < \theta < 151^\circ$ angular coverage. Conical-shaped end-plates are used to keep the forward and background acceptance open where are covered by the FDCs, the BDCs, and the PID counters. The outer radius is 530 mm and the inner radius is 150 mm, with the longest wire length of 2.2 m. To obtain a good tracking efficiency and momentum resolution for low- p_t tracks, the CDC is designed to have thin and thick CFRP cylinders as the inner and outer wall, respectively.

The CDC is composed of 17 tracking layers which are grouped into 7 super-layers. The cell of all tracking layers is small hexagonal shape with a typical drift length of 9 mm. Table 1 gives the conceptual parameter of the wire configuration. The 8 stereo

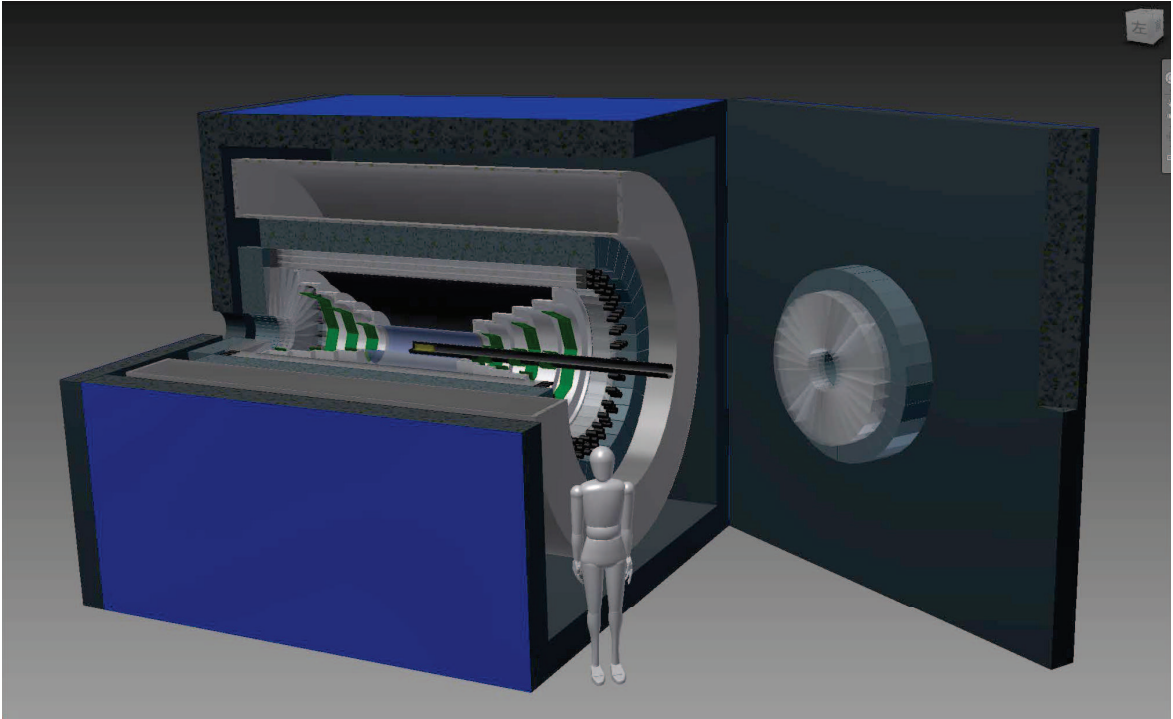


Figure 9: Conceptual design of the CDS (3D model).

layers tilted by about 3.5° are used to obtain longitudinal position information. The number of readout channels is ~ 2150 .

We plan to use gold-plated tungsten of $30 \mu\text{m}$ ϕ for the sense wires and gold-plated aluminum of $100 \mu\text{m}$ ϕ for the field and guard wires, which are supported by feedthroughs with a bushing inserted at the end. The drift gas is 1 atm of mixed argon (50%) - ethane (50%). A high voltage is applied to the field and guard wires, and the sense wires are kept at ground potential. As the readout electronics, we use a preamp card with ASDs (SONY-CXA3653Q, $\tau = 16 \text{ ns}$) and Hadron Universal Logic (HUL) boards. The expected transversed-momentum resolution is $5.3 \% p_t \oplus 0.5 \% / \beta$ corresponding to $\sim 3\%$ on 500 MeV/c particles.

3.3.3 Vertex Fiber Tracker (VFT)

The high-resolution vertex determination is indispensable to discriminate between the signals and backgrounds with event topology such as distance of closest approach method: for instance, the $\pi^\pm \Sigma^\mp \rightarrow \pi^+ \pi^- n$ decays would be separated clearly together with the invariant mass and decay vertex topology. With only the CDC, the vertex resolution of the beam direction (z-direction) is expected to be $\sim 1 \text{ cm}$, while that of the radius direction (r-direction) is a few mm. This is due to small tilt angles of the stereo layers which is limited by the feedthrough layout. By introducing the VFT,

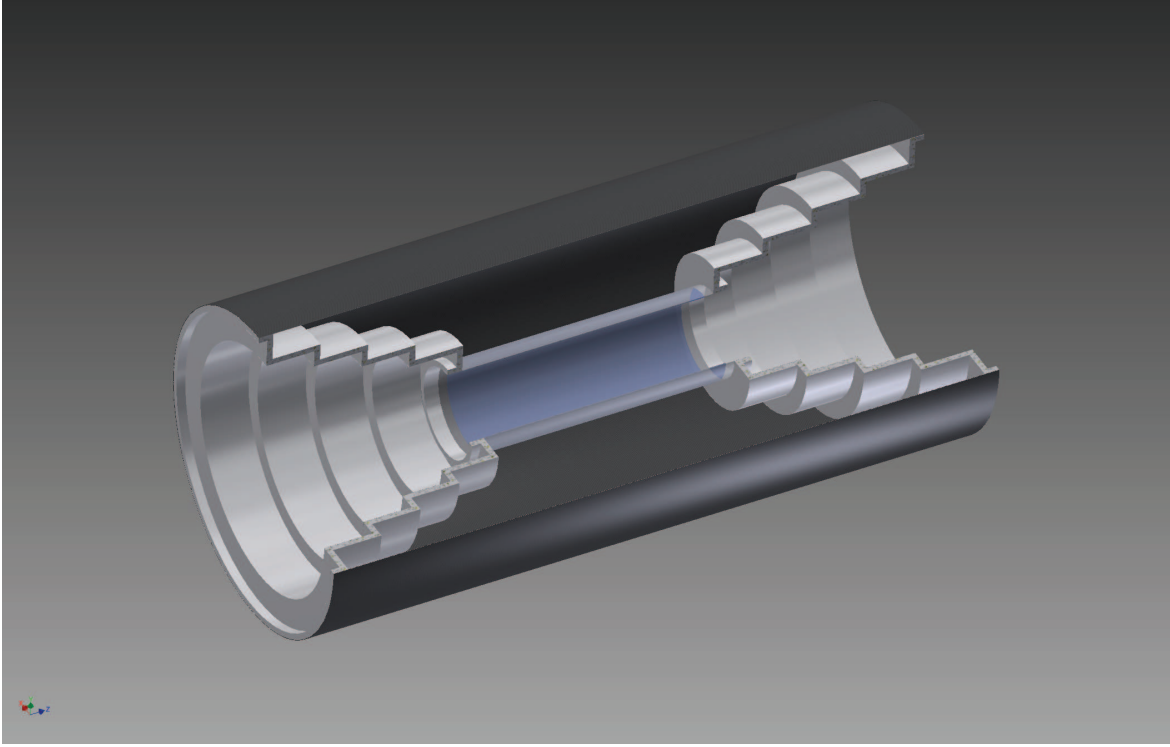


Figure 10: Conceptual design of the CDC).

Table 1: Conceptual parameter of the wire configuration of the CDC.

Super layer	Layer	Wire direction	Radius (mm)	Cell width (degree)	Cell width (mm)	Stereo angle (degree)	Signal channel per layer
A1	1, 2, 3	X, X' X	190 - 230	5.00	~ 18.0	0	72
U1	4, 5	U, U'	250 - 300	3.60	~ 18.5	~ ± 3.5	100
V1	6, 7	V, V'	320 - 360	3.00	~ 18.0	0	120
A2	8, 9, 10	X, X' X	380 - 430	2.25	~ 17.0	~ ± 3.5	160
U2	11, 12	U, U'	450 - 490	2.00	~ 16.5	0	180
V2	13, 14	V, V'					
A3	15, 16, 17	X, X' X					

the vertex resolution in the beam direction will be improved to a few mm with a combination of the CDC tracking information.

The VFT is installed on the outer wall of the target chamber ($r \sim 80$ mm). We plan to use 4 layers of 1 mm ϕ scintillating fibers having $UU'VV'$ configuration. In the U and V layers, the fibers are tilted by ± 45 degrees. For readout, the system developed for the fiber-tracker system in the E50 experiment will be used. The total readout channel is ~ 2000 ($= \sim 500 \times 4$).

3.3.4 Backward and Forward Drift Chambers (BDCs/FDCs)

The BDCs and FDCs are installed just upstream and downstream of the target, respectively, aiming to reconstruct backward- and forward-going particles which cannot be detected by the CDC. Each chamber is a set of octagonal planar wire drift chambers, which is composed of 3 modules with different size depending on the distance from the target.

The BDCs are placed 0.5 m, 0.8 m, and 1.1m upstream from the target with the size of 30 cm, 50 cm, 70 cm inscribed circle diameters, respectively. Each chamber consists of 8 layers with an $XX'YY'XX'YY'$ configuration, whose layer contains 32, 64, 96 sense wires with a drift length of ~ 4 mm, respectively. The FDCs are placed 0.5 m, 0.8 m, and 1.1m downstream from the final focus, and are almost the same structure as the BDCs but the centers of the chambers is cut out not to interfere with the target chamber. The chamber gas is an argon (80%) - isobutane (20%) mixture, and we use the same readout electronics as the CDC, *i.e.*, the ASD preamp cards and the HUL boards.

3.3.5 Charged-particle Hit Counter (CHC)

In the proposed experiment, the neutral particle detections is a key of the systematic studies of the kaonic nuclei. To realize the efficient data accumulation of both charged and neutral particles, online counting of the both charged- and neutral-particle multiplicity is essential. For this purpose, we install a thin segmented plastic scintillation counter as the CHC for the trigger counter. The charged-particle multiplicity is obtained with the CHC, while the neutral-particle multiplicity is obtained with the combination of the CHC-veto and NC/ECAL information.

The CHC is divided into a cylindrical barrel part (barrel CHC) and the two facing endcap sections (endcap CHCs), which is located at just front of the NC. Each of the barrel and endcap CHCs has a thickness of 3 mm whose scintillation light is read out using wave-length shifting fibers and MPPCs. Segmentation of the CHC is the same as that of the NC and ECAL as described below.

3.3.6 Neutron Counter (NC)

The NC is an array of segmented plastic scintillation counters used for the neutron detection. The first layer of the NC is also used for the charged-particle identification

as a hodoscope counter. The NC is divided into a cylindrical barrel part (barrel NC) and the two facing endcap sections (endcap NCs). Each of the barrel and endcap NCs has a thickness of 15 cm divided into three layers. The expected neutron detection efficiency is 15% \sim 45% which depends on the neutron momentum.

The barrel NC is located at a radius of 530 mm from the beam axis covering a polar angle range from 29 to 151 degrees. The barrel NC consists of 32 modules in a layer whose scintillators are made of Eljen EJ-200 with dimensions of 2.6 m in length, \sim 120 mm in width, and 50 mm in thickness. The scintillation light is transferred through light guides to a pair of Hamamatsu R7761 fine-mesh 19-dynode photomultipliers 1.5 inches in diameter.

The endcap NCs are mounted on the each endcap of the solenoid magnet together with a endcap ECAL described in the next subsection, which cover a polar angle range from 7(160) to 20(173) degrees. The endcap NCs consist of 32 trapezoid modules in a layer whose scintillators are made of Eljen EJ-200 with dimensions of 400 mm in length, 30 -100 mm in width, and 50 mm in thickness. We plan to use MPPC arrays to read out the scintillation light from the both sides of the module, by assembling 4 \sim 10 pieces of 6 mm \times 6 mm MPPCs.

3.3.7 Electromagnetic Calorimeter (ECAL)

The ECAL is a sampling-type calorimeter used for photon energy measurement. The ECAL is divided into a cylindrical barrel part (barrel ECAL) and the two facing endcap sections (endcap ECALs). Each of the barrel and endcap ECALs has a thickness of 23 cm. We plan to construct the ECAL with a lead - scintillating-fiber calorimeter developed for the KLOE experiment [46] or a lead - scintillator-slab with wave-length shifting fibers calorimeter used in such as the CLAS experiment [47]. In each case, \sim 15 radiation length is required to precisely reconstruct the photon energy with $\Delta E/E \sim 6\%/\sqrt{E(GeV)}$.

The barrel ECAL is located at a radius of 680 mm from the beam axis covering a polar angle range from 32 to 148 degrees. The barrel ECAL consists of 32 modules with dimensions of 2.9 m in length, 130 - 170 mm in width. The endcap ECALs are mounted on the each endcap of the solenoid magnet together with a endcap NC, which cover a polar angle range from 7(158) to 22(173) degrees. The endcap ECALs consist of 32 trapezoid modules with dimensions of 500 mm in length, 30 -130 mm in width.

3.4 Trigger

A dedicated hardware trigger is developed to meet experimental requirements. The kaon beam trigger is constructed with the same procedure as the previously performed experiments at the K1.8BR beamline. The elementary beam trigger is constructed by coincidence signals from the beamline counters, and the kaon beam trigger is selected from the beam trigger by using the kaon identification counter (*i.e.*, the aerogel Cherenkov counter).

To select an event associated with the kaonic nuclei production, we use the simplest charged-multiplicity trigger implemented in hardware level with the CHC. The number of the CHC hits (CHC_n) is selected according to the target species. For example, CHC_3 is used for the $K^- \text{ } ^4\text{He} \rightarrow \text{“}K^- ppn\text{”}$ $n \rightarrow \Lambda d \rightarrow \pi^- pd$, where three charged particles detection is required. In addition, we introduce the neutral-multiplicity trigger to select neutron and/or γ -ray in online level. We implement the neutral trigger using a FPGA logic board of the HUL, with the CHC and the NC/ECAL hit information. The CHC is used as a veto counter for neutral particles, and the neutral trigger is constructed by taking coincidence between the veto-CHC and NC/ECAL hits in the same ϕ -direction.

By combining the charged- and neutral-multiplicity triggers, we can realize any dedicated trigger for from the $\bar{K}N$ to $\bar{K}NNNN$ measurements. We use the Hadron DAQ system with the HUL as the online data acquisition system, whose maximum accumulation rate has been confirmed to reach to ~ 10 k events per spill with more than 90% DAQ efficiency. In the proposed experiment, the expected trigger rate of the main trigger (for example of $\text{“}K^- ppn\text{”}$ – main trigger is CHC_3) is a few kHz by taking into account the previous experiments. Therefore, trigger rate is controllable according to the physics purpose by using the combination of the charged- and neutral-multiplicity triggers.

3.5 Summary of Improvements of the Detector System

In this section, we discuss improvement points of the new proposed experimental setup compared with the previous E15 setup. Two major upgrades are planned, namely, the beamline spectrometer and CDS. Details are discussed as follows.

3.5.1 Beamline Spectrometer

We propose to improve the existing beamline of the K1.8BR which was constructed to be dedicated to the (K^-, N) measurements with forward neutron and proton counter arrays. For the E15 experiment, we installed a dipole magnet (D5) at just upstream of the final focus point by modifying the original design of the K1.8BR beamline optics. This installation was aimed to achieve the forward neutron TOF resolution of ~ 10 MeV/ c^2 with 15 m TOF length between a T0 counter and the forward neutron counter array. As a result, the beamline length became long (~ 3.7 m), which resulted a decrease of available kaon beam.

In the improvement we propose, the D5 magnet is removed so that the available kaon yield is maximized. Since the beam trajectory is drastically changed by the removal, the beam dump is also required to be moved along the beam direction. Therefore, we request to rearrange the K1.8BR experimental area as shown in Fig. 6. At the modified experimental area, the beam dump is moved from the west side of the hadron hall currently installed to the north side.

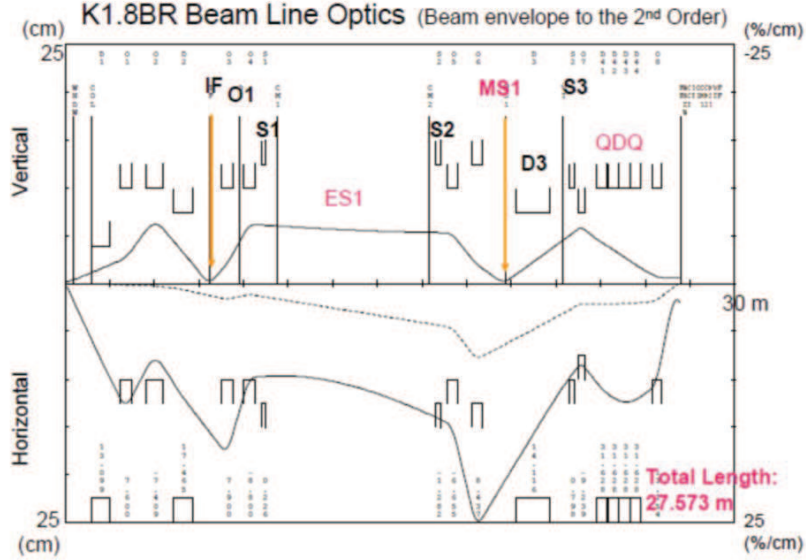


図 8 : K1.8BR ビームエンベロープ

Figure 11: Beamline optics of the improved K1.8BR beamline.

For future experiments performed at the K1.8BR beamline, the experimental area must be as large as possible. This is because we are planning to install a forward spectrometer composed of a large dipole magnet and a tracking system to expand the scope of experimental programs at K1.8BR. For instance, we can perform an experiment dedicated to measure a forward going nucleon from the (K^-, N) reactions with decay coincidence, such as the original proposal of the E15 experiment. Furthermore, we can realize a so-called K^0 spectrometer using the proposed system, which enable us to investigate neutron-rich hypernuclei with the (π^-, K^0) reactions.

The evaluated beam optics with the new beamline setup is shown in Fig. 11. The shortening of the beamline from the current configuration is essential for experiments using the low momentum kaon beam. It should be noted that, because the size of the new CDS becomes larger than the previously used CDS as described in Sec. 3.3, the final focusing point is shifted to the downstream of the beamline by ~ 1.2 m, *i.e.*, the shortening length is effectively ~ 2.5 m. As for the improvement of the beam focus, we adopt a conservative value of the fiducial-volume-selection efficiency of 0.65: the value was obtained at the predecessor experiments in which the same target cell was used as the proposed experiment. This is because the beam size of the secondary beamline strongly depends on beamline tuning. There are many uncertainties to reproduce the beam condition by the simulation codes of TRANSPORT and TURTLE, even though at the existing beamline of the K1.8BR. Thus, the available kaons on target are conservatively estimated to increase ~ 1.4 times, which corresponds to 3.2×10^5

kaons on target per spill at the beam power of 90 kW with 5.2 s repetition cycle [‡].

3.5.2 CDS

We are planning to construct the new CDS to reach unreachable investigations at the predecessor experiment. The existing CDS used for E15 consists of a solenoid magnet, a cylindrical wire drift chamber (CDC), and a cylindrical detector hodoscope (CDH) with 3 cm plastic scintillators. The system has a solid angle coverage of 59%. To determine the isospin and parity of the kaonic nuclei, one need to investigate the production and decay topology with 4π acceptance. In the “ K^-pp ” case of E15, we found the hardness of the decay asymmetry measurement in the Λp decay and Λ decay itself due to a lack of the CDS acceptance in the forward and backward directions.

The new large CDS having $\sim 4\pi$ acceptance allow us to perform such measurement with less uncertainties of the determination. Details of the experimental approach toward spin-parity determination of the $\bar{K}NN$ state will be demonstrated in the other proposal shortly. In this proposal, we demonstrate an improvement of the CDS acceptance using the $K^- + {}^3\text{He} \rightarrow \Lambda pn$ channel which has been well studied in the E15 experiment. Figure 12 shows a comparison of the detector acceptance between the existing CDS (E15-CDS) and the newly constructed CDS (new-CDS). The acceptances for the Λp detection with each the CDS are evaluated with a full Monte-Carlo simulation whose details are described in Sec. 4. The detector acceptance of the new CDS is drastically improved as clearly seen in the figure. The enlargement of the acceptance is quite essential for the systematic investigation of kaonic nuclei to efficiently detect particles in the final state and to specify the reaction channel in unambiguous manner.

The CDS upgrade with capability of neutral particle detection also enables us to measure the various decay modes, *i.e.* not only non-mesonic decay channels but also mesonic decay channels of the kaonic nuclei. In the $\Lambda(1405)pn$ analysis with the ${}^3\text{He}(K^-, \pi^\pm \Sigma^\mp p)n$ measurement described in Sec. 1.1, we suffered from huge backgrounds mainly originated from neutron misidentification. This is due to poor neutron detection efficiency and small acceptance coverage in the forward and backward regions. Particles not detected with the CDC and CDH generate secondary particles in reactions between the solenoid-magnet yoke, which subsequently make background hits on the CDH resulting fake neutron events. We have found that this poor neutron efficiency and the small acceptance make quite difficult to investigate the “ K^-pn ” state – the isospin partner of “ K^-pp ” which is expected to decay into Λn channel.

Thus, it is critical to realize the higher neutron efficiency with wider acceptance for the systematic measurements of the kaonic nuclei. In the proposed experiment, we introduce thicker scintillators of 150 mm thickness covering wide area, as the neutron detector of the CDS. We can achieve ~ 5 times larger neutron-detection efficiency than that of the existing CDS. This improvement enables us to identify a neutron with small ambiguity, and thus to investigate the kaonic nuclei systematically.

[‡] 2.0×10^5 (Run85, 2020 @ 51kW) $\times 0.65$ (fiducial volume selection) $\times 1.4$ (beamline length) $\times 90/51$ (beam power) $\sim 3.2 \times 10^5$.

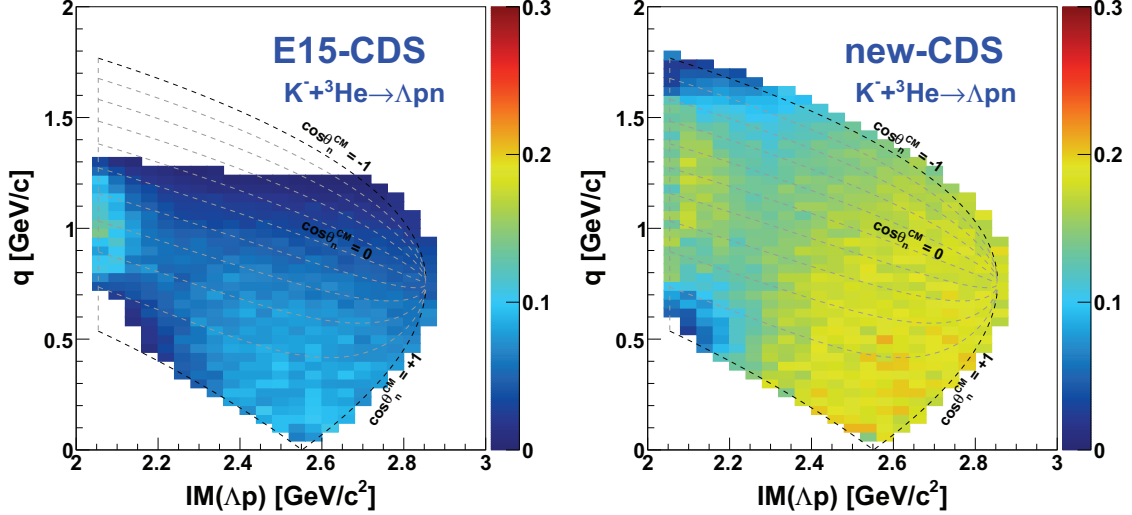


Figure 12: Detector acceptance for the Λp detection with the CDS in the $K^- + {}^3\text{He} \rightarrow \Lambda p n$ reaction. The left figure shows the acceptance with the existing CDS (E15-CDS), and the right shows that with the newly constructed CDS (new-CDS). The relation between q and $\cos(\theta_n^{CM})$ is also represented, where $\cos(\theta_n^{CM})$ denotes the polar angle of the missing neutron in the center-of-mass frame of the $K^- + {}^3\text{He}$ reactions.

4 Yield Estimation and Expected Spectrum

4.1 Yield Estimation

In the $K^- + {}^3\text{He} \rightarrow \Lambda p n$ measurement, we obtained the production cross section of the “ $K^- pp$ ” as $\sigma_{Kpp}^{tot} \cdot BR(\Lambda p) \sim 10 \mu\text{b}$ [34]. To estimate the expected yield of the “ $K^- ppn$ ”, we assume that the “ $K^- ppn$ ” cross section in the $K^- + {}^4\text{He} \rightarrow X + n$ reaction is the same of the “ $K^- pp$ ” $\rightarrow \Lambda p$, *i.e.*,

$$\begin{aligned} \sigma_{Kppn}^{tot} \cdot BR(\Lambda d) &\sim 10 \mu\text{b}, \\ \sigma_{Kppn}^{tot} \cdot BR(\Lambda pn) &\sim 10 \mu\text{b}. \end{aligned}$$

As for the decay branch of the $K^- ppn$ state with a deuteron, it may be a useful to refer to the absorption of stopped K^- on a ${}^4\text{He}$ nucleus. In the reaction, decay fraction to $\Sigma^- pd$ or $\Sigma^- ppn$ is known to be almost the same [48]. By analogy with this result, we adopt an assumption that the branching ratio of the Λd decay from the $K^- ppn$ state would be the same as that of the Λpn decay.

The detector acceptance of the CDS (Ω_{CDS}) is evaluated with a full detector simulation by assuming the obtained event distributions in E15. For the simulation, the GEANT4 toolkit ver.10.2.3 with the “QGSP_BERT_HP” physics list [49] is used. The

Table 2: Estimated yields normalized by 1 G (10^9) K^- beam, for typical expected decay modes. The binding energies of ~ 50 MeV and widths of ~ 100 MeV are assumed for each bound state.

	K^-pp (^3He)		K^-pn (^3He)	K^-ppn (^4He)	K^-ppn (^4He)
decay mode	Λp		Λn	Λd	Λpn
$\sigma^{tot} \cdot BR$	10 μb		assumed to be 10 μb		
N_{beam}	10^9				
spectrometer	E15-CDS		new-CDS		
N_{target}	1.92×10^{23} *		1.73×10^{23} *	2.58×10^{23}	
ϵ_{beam}	0.55				
ϵ_{DAQ}	0.74		0.9		
$\epsilon_{trigger}$	0.93				
$\epsilon_{fiducial}$	0.65				
Ω_{CDS}	0.12	0.28	0.085	0.27	0.077
ϵ_{CDS}	0.6		0.3	0.6	0.3
N	33	120	18	170	25

momentum dependence of the neutron-detection efficiency with the NC is also simulated with the GEANT4 physics process.

The estimated yields for each channel normalized by 1 G (10^9) K^- beam are summarized in Tab. 2, where those for the “ K^-pp ” and “ K^-pn ” states are also shown as a reference. We assume the similar spectrum shape of the observed “ K^-pp ” in E15 for each bound state, with the binding energies of ~ 50 MeV and widths of ~ 100 MeV. The CDS acceptance of Ω_{CDS} is obtained for the exclusive reconstruction of $^3/4\text{He}(K^-, \Lambda p/\Lambda n/\Lambda d/\Lambda pn)N$ where the missing N is identified from the missing mass. The yields are calculated using the following equation:

$$\begin{aligned}
 N &= \sigma \times N_{beam} \times N_{target} \times \epsilon, \\
 \epsilon &= \epsilon_{DAQ} \times \epsilon_{trigger} \times \epsilon_{beam} \times \epsilon_{fiducial} \times \Omega_{CDS} \times \epsilon_{CDS},
 \end{aligned}$$

where

N : expected yield,

*In the E15 experiment, we used the siphon-type refrigerator system, where 1.30 K operation was realized – density of liquid ^3He is 0.081 g/cm³. During the operation of the refrigerator system, we needed ^4He refrigerant refill work for 1 hour everyday. Now we use the new target system with the pulse tube refrigerator system which does not need ^4He refrigerant. On the other hand, because achievable temperature is a bit high of 2.7 K (density of 0.070 g/cm³) with the new system, the available number of target is decreased. As for the ^4He liquefaction used in this proposed experiment, the available number of target is not changed because the target density is almost the same between 1.30 K and 2.7 K.

Table 3: Estimated yields under the MR beam power of ~ 90 kW with 5.2 s repetition cycle. In the list of the E15-2nd experiment, we show the results of Run#65 conducted in 2015, whose obtained yield is consistent with the calculated yield with the E15-2nd condition.

	K^-pp (^3He)	K^-pn (^3He)	K^-ppn (^4He)	K^-ppn (^4He)
decay mode	Λp	Λn	Λd	Λpn
$\sigma^{tot} \cdot BR$	$10 \mu\text{b}$	assumed to be $10 \mu\text{b}$		
experiment	E15-2nd	exp. in near future	proposed exp.	
MR beam power	42 kW	90 kW		
beam-time duration	1 month	3 weeks		
accelerator up-time	0.89	0.9		
# of K^- beam	62×10^9	155×10^9		
# of K^- on target	40×10^9	100×10^9		
# of expected yield	1.7×10^3	13×10^3	2.0×10^3	2.8×10^3

- σ : cross section including the branching ratio,
- N_{beam} : number of the beam kaons,
- N_{target} : number of the target particles,
- ϵ : total experimental efficiency,
- ϵ_{DAQ} : DAQ efficiency,
- $\epsilon_{trigger}$: trigger efficiency,
- ϵ_{beam} : analysis efficiency of the beam kaons,
- $\epsilon_{fiducial}$: efficiency of fiducial volume selection,
- Ω_{CDS} : detector acceptance of the CDS,
- ϵ_{CDS} : analysis efficiency of the CDS.

In the calculation of N_{target} , fiducial volume length of 11.8 cm is adopted, which was set to the E15-2nd analysis. We assume the same parameters obtained and evaluated in the analysis of the predecessor experiments at the K1.8BR: $\epsilon_{beam} = 0.55$, $\epsilon_{trigger} = 0.93$, $\epsilon_{fiducial} = 0.65$, $\epsilon_{CDS} = 0.6$ for $\Lambda p/\Lambda d$ channels, and $\epsilon_{CDS} = 0.3$ for $\Lambda n/\Lambda pn$ channels whose decay neutron is detected with the NC of the CDS (or the CDH of the E15-CDS).

At the improved K1.8BR beamline, we expect the kaons on target of 3.2×10^5 per spill with the momentum of 1.0 GeV/c, under the MR beam power of ~ 90 kW with 5.2 s repetition cycle. Table 3 shows the estimated yields with 3 weeks beam time under assumption of 90% accelerator up-time – 100 G kaons on target (155 G beam kaon without fiducial volume selection). Compared to the obtained “ K^-pp ” yield at

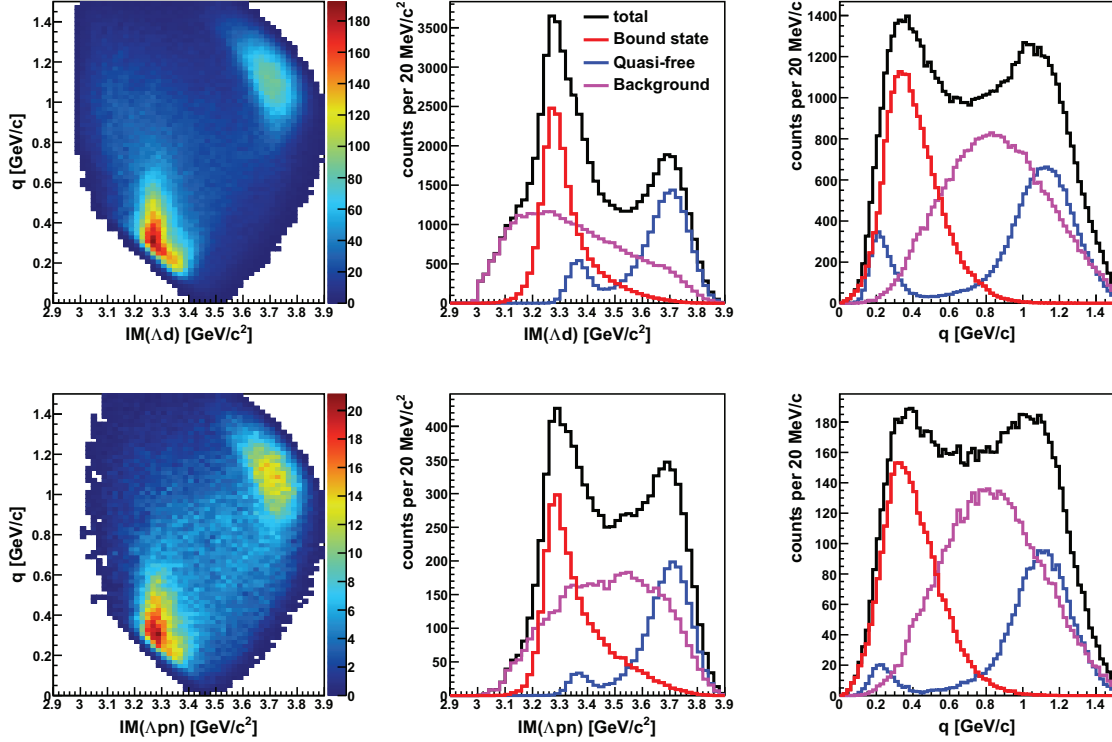


Figure 13: Expected spectra of the (top) Λd and (bottom) Λpn in the $K^- + {}^4\text{He} \rightarrow \Lambda d + n$ and $\Lambda pn + n$ final state with 100 G kaons on target, respectively. Here, we assume the cross section of the K^-ppn , quasi-free, and background of $10 \mu\text{b}$, $10 \mu\text{b}$, and $20 \mu\text{b}$, respectively, based on the E15 results.

the E15-2nd, we expect ~ 10 times larger statistics of “ K^-ppn ” $\rightarrow \Lambda d$ accumulation, and, the same statistical order of the “ K^-ppn ” $\rightarrow \Lambda pn$.

4.2 Expected Spectrum

Figure 13 shows the expected spectra of the $K^- {}^4\text{He} \rightarrow \Lambda dn$ and the Λpnn final states with 100 G kaons on target corresponding to 3 weeks data taking under 90 kW beam power. For the K^-ppn state in the figures, we assume the similar distribution of the “ K^-pp ” observed in E15: the binding energy of ~ 50 MeV, the width of ~ 100 MeV, and the Gaussian form factor of ~ 400 MeV/c with $10 \mu\text{b}$ ($\sigma \cdot BR$). As for the quasi-free process and the broad background, we also used the similar parameters obtained in the $K^- + {}^3\text{He} \rightarrow \Lambda pn$ final state in E15.

The spectra for each process are generated using the Geant4 simulation, in which we assume the same resolution of the existing CDS to reconstruct the simulated tracks $- 5.3\% \times p_t \oplus 0.5\%$ for charged particles and $\sim 10\% \times p \oplus 7\%$ for a neutron. In the

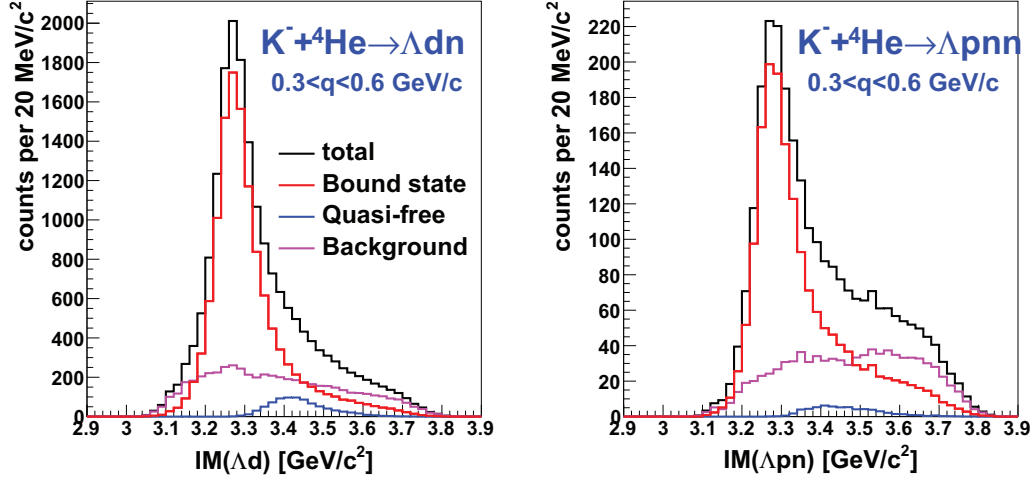


Figure 14: Expected invariant mass spectra of the (left) Λd and (right) Λpn in the region of $0.3 < q < 0.6$ GeV/ c , which are obtained from Fig. 13.

assumed conditions, the bound states are clearly identified not only in the invariant mass spectra but also in the $q - IM$ distribution, which is the most important feature of the proposed experiment. By investigating the specific structures in the $q - IM$ distribution, we can kinematically identify the signal of the bound state. Figure 14 shows a demonstration of the signal enhancement by selecting the momentum transfer of $0.3 < q < 0.6$ GeV/ c . In the region, we expect that the bound state is clearly separated from the quasi-free process, as we shown in Fig. 2 using the E15 data of the Λpn final state. The cross-section of the K^-ppn decays can be determined if those cross sections are more than $\sim \mu b$, where we assume the backgrounds are same as that assumed in Fig 13.

5 Schedule and Beam Time Plan

Figure 15 shows the time line of the preparation for the proposed experiment. We would like to perform the proposed experiment in 2023, thus the detector system required for the experiment has to be ready in 2022. The modification of the K1.8BR experimental area is hopefully conducted in the summer of 2021, whose cost is expected to be covered by KEK budget. The design works of the main part of the CDS, *i.e.* the super-conducting solenoid, the CDC, and the NC, are going on and will be completed in 2020. Then the construction of the main part will be conducted in 2021, and after the detector test and commissioning those system will be integrated at J-PARC in 2022. The backward and forward drift chambers will be also designed and constructed by the middle of 2022. After commissioning of the whole detector system with cosmic

	2020			2021				2022				2023				2024											
	Q2	Q3	Q4	Q1	Q2	Q3	Q4	Q1	Q2	Q3	Q4	Q1	Q2	Q3	Q4	Q1	Q2	Q3	Q4								
Magnet	design	purchase (S.C. wires)		construction				test and commissioning				integration				comm. run				physics run				analysis, publication			
VFT	design																										
GDC																											
Backward DC																											
Forward DC				design and construction				test and comm.																			
Chamber Readout				R&D		production																					
BHT				construction				test and commissioning																			
CHC	design			purchase				assembly				test and commissioning															
NC																											

Figure 15: Schedule of the preparation for the proposed experiment.

ray in the middle of 2022, the experiment will be ready in the beginning of 2023.

Table 4 shows a summary of the requested beam time. At around 2023, the MR beam power will increase by ~ 90 kW. We expect the negative-kaon beam yield of ~ 320 k per spill with the momentum of 1.0 GeV/ c at the K1.8BR beamline. In the beam time plan, we do the detector commissioning with actual kaon beam for one week as a beginning, where we optimize the detector operation under the same condition of the production run. After completion of the commissioning, we continue the performance study run with the liquid H_2 target for one week to confirm detector performance by demonstrating $K^0 \rightarrow \pi^+\pi^-$, $\Lambda \rightarrow \pi^-p$ and $\Sigma^\pm \rightarrow \pi^\pm n$ reconstruction with the CDS. The one week data taking corresponds to ~ 33 G K^- on target (50 G K^- beam) which is ~ 10 times larger than that accumulated in the E15 H_2 run in 2015. Then the production run with liquid 4He target is carried out for three weeks. We expect ~ 100 G kaons on target with the 90% machine up-time, which is ~ 2.5 times larger than that accumulated in the E15 3He run in 2015.

6 Cost Estimation

The total cost to construct the new system is estimated to be ~ 600 M JPY, which is summarized in Tab. 5. Most of the cost will be covered by the budget of "Grand-In-Aid for Specially Promoted Research by MEXT" and RIKEN internal budget.

The cost includes constructions of the superconducting solenoid magnet, the VFT,

Table 4: Summary of the beam-time plan.

Duration at 90 kW	# of K^- on target	Experimental target	Purpose of the experiment
1 week	–	–	commissioning
1 week	33 G	Liquid H_2	performance study
3 weeks	100 G	Liquid 4He	$\bar{K}NNN$ production

Table 5: Cost estimation to construct the new system.

Item	Cost [JPY]	Budget Source
Super-conducting Solenoid Magnet	200 M	Grant-In-Aid
VFT	20 M	Grant-In-Aid
CDC	130 M	Grant-In-Aid
Read-out system for CDC	30 M	Grant-In-Aid
Backward DCs	30 M	RIKEN int. budget / Grant-In-Aid
Forward DCs	30 M	RIKEN int. budget / Grant-In-Aid
Read-out system for DCs	20 M	RIKEN int. budget / Grant-In-Aid
BHT	10 M	RIKEN int. budget / Grant-In-Aid
CHC	10 M	RIKEN int. budget / Grant-In-Aid
Scintillator for Barrel NC	30 M	Grant-In-Aid
PMTs for Barrel NC	20 M	Grant-In-Aid
Scintillator for Endcap NC	15 M	Grant-In-Aid
Read-out system for MPPCs	10 M	Grant-In-Aid
Total	~ 600 M	

the CDC, the BDCs and FDCs, the NCs, the CHC, the BHT, and those read-out systems. Fine-mesh PMTs used for the previous experiment are reused as a part of the barrel NC's read-out to reduce the total cost. The ECAL system, whose cost is not included in the current estimation, is expected as an international contribution from the INFN-LNF and SMI with their construction know-how of the KLOE system. The conceptual design work for the ECAL is just started, and the construction cost of the ECAL is estimated to be ~ 700 M JPY when we adopt the design of the KLOE type calorimeter. Therefore, experimental projects to use the ECAL is assigned to be the second stage of the project at the K1.8BR beamline.

References

- [1] M. Iwasaki *et al.* *Phys. Rev. Lett.* **78** (1997) 3067.
- [2] G. Beer *et al.* *Phys. Rev. Lett.* **94** (2005) 212302.
- [3] M. Bazzi *et al.* *Phys. Lett.* **B704** (2011) 113.
- [4] A. D. Martin *Nucl. Phys.* **B179** (1981) 33.
- [5] Y. Nogami *Phys. Lett.* **7** (1963) 288.
- [6] Y. Akaishi and T. Yamazaki *Phys. Rev.* **C65** (2002) 044005.
- [7] T. Yamazaki and Y. Akaishi *Phys. Lett.* **B535** (2002) 70.
- [8] N. V. Shevchenko, A. Gal, and J. Mares *Phys. Rev. Lett.* **98** (2007) 082301.
- [9] N. V. Shevchenko, A. Gal, J. Mares, and J. Révai *Phys. Rev.* **C76** (2007) 044004.
- [10] Y. Ikeda and T. Sato *Phys. Rev.* **C76** (2007) 035203.
- [11] A. Doté, T. Hyodo, and W. Weise *Nucl. Phys.* **A804** (2008) 197.
- [12] Y. Ikeda and T. Sato *Phys. Rev.* **C79** (2009) 035201.
- [13] S. Wycech and A. M. Green *Phys. Rev.* **C79** (2009) 014001.
- [14] A. Doté, T. Hyodo, and W. Weise *Phys. Rev.* **C79** (2009) 014003.
- [15] Y. Ikeda, H. Kamano, and T. Sato *Prog. Theor. Phys.* **124** (2010) 533.
- [16] N. Barnea, A. Gal, and E. Z. Liverts *Phys. Lett.* **B712** (2012) 132.
- [17] M. Bayar and E. Oset *Phys. Rev.* **C88** (2013) 044003.
- [18] S. Maeda, Y. Akaishi, and T. Yamazaki *Proc. Jpn. Acad.* **B89** (2013) 418.
- [19] J. Révai and N. V. Shevchenko *Phys. Rev.* **C90** (2014) 034004.
- [20] A. Doté, T. Inoue, and T. Myo *Prog. Theor. Exp. Phys.* **2015** (2015) 043D02.
- [21] T. Sekihara, E. Oset, and A. Ramos *Prog. Theor. Exp. Phys.* **2016** (2016) 123D03.
- [22] S. Ohnishi *et al.* *Phys. Rev.* **C95** (2017) 065202.
- [23] A. Doté, T. Inoue, and T. Myo *Phys. Rev.* **C95** (2017) 062201.
- [24] A. Doté, T. Inoue, and T. Myo *Phys. Lett.* **B784** (2018) 405.

- [25] M. Agnello *et al.* *Phys. Rev. Lett.* **94** (2005) 212303.
- [26] T. Yamazaki *et al.* *Phys. Rev. Lett.* **104** (2010) 132502.
- [27] Y. Ichikawa *et al.* *Prog. Theor. Exp. Phys.* **2015** (2015) 021D01.
- [28] O. Vazquez Doce *et al.* *Phys. Lett.* **B758** (2016) 134.
- [29] R. Del Grande *et al.* *Eur. Phys. J.* **C79** (2019) 190.
- [30] G. Agakishiev *et al.* *Phys. Lett.* **B742** (2015) 242.
- [31] A. O. Tokiyasu *et al.* *Phys. Lett.* **B728** (2014) 616.
- [32] T. Hashimoto *et al.* *Prog. Theor. Exp. Phys.* **2015** (2015) 061D01.
- [33] Y. Sada *et al.* *Prog. Theor. Exp. Phys.* **2016** (2016) 051D01.
- [34] S. Ajimura *et al.* *Phys. Lett.* **B789** (2019) 620.
- [35] T. Kishimoto *Phys. Rev. Lett.* **83** (1999) 4701.
- [36] T. Sekihara, E. Oset, and A. Ramos *JPS Conf. Proc.* **26** (2019) 023009.
- [37] J. M. M. Hall *et al.* *Phys. Rev. Lett.* **114** (2015) 132002.
- [38] T. Yamazaki and Y. Akaishi *Phys. Rev.* **C76** (2007) 045201.
- [39] S. Ohnishi, Y. Ikeda, H. Kamano, and T. Sato *Phys. Rev.* **C88** (2013) 025204.
- [40] M. Sato *et al.* *Phys. Lett. B* **659** (2008) 107.
- [41] H. Yim *et al.* *Phys. Lett. B* **688** (2010) 43.
- [42] M. Agnello *et al.* *Phys. Lett. B* **654** (2007) 80.
- [43] N. Herrmann *et al.* *Proc. EXA05 Conference ISBN 3-7001-3616-1* (2005) 73.
- [44] K. Agari *et al.* *Prog. Theor. Exp. Phys.* **2012** (2012) 02B009.
- [45] K. Agari *et al.* *Prog. Theor. Exp. Phys.* **2012** (2012) 02B011.
- [46] M. Adinolfi *et al.* *Nucl. Instrum. Meth.* **A482** (2002) 364.
- [47] M. Amarian *et al.* *Nucl. Instrum. Meth.* **A460** (2001) 239.
- [48] P. Katz *et al.* *Phys. Rev. D* **1** (1970) 1267.
- [49] J. Allison *et al.* *Nucl. Instrum. Meth.* **A835** (2016) 186.